ORNL/TM-2016/93

Light Water Reactor Sustainability Program

Thermodynamic and Kinetic Model Development of Thermal Segregation of Phosphorus in Iron, Fe-Cr and Fe-Ni Systems – Towards the Development of a Comprehensive Solute Segregation Model

March 2016

U.S. Department of Energy

Office of Nuclear Energy

DOCUMENT AVAILABILITY

Reports produced after January 1, 1996, are generally available free via US Department of Energy (DOE) SciTech Connect.

Website http://www.osti.gov/scitech/

Reports produced before January 1, 1996, may be purchased by members of the public from the following source:

National Technical Information Service
5285 Port Royal Road
Springfield, VA 22161
Telephone 703-605-6000 (1-800-553-6847)
TDD 703-487-4639
Fax 703-605-6900
E-mail info@ntis.gov
Website http://www.ntis.gov/help/ordermethods.aspx

Reports are available to DOE employees, DOE contractors, Energy Technology Data Exchange representatives, and International Nuclear Information System representatives from the following source:

Office of Scientific and Technical Information
PO Box 62
Oak Ridge, TN 37831
Telephone 865-576-8401
Fax 865-576-5728
E-mail reports@osti.gov
Website http://www.osti.gov/contact.html

DISCLAIMER

This information was prepared as an account of work sponsored by an agency of the U.S. Government. Neither the U.S. Government nor any agency thereof, nor any of their employees, makes any warranty, expressed or implied, or assumes any legal liability or responsibility for the accuracy, completeness, or usefulness, of any information, apparatus, product, or process disclosed, or represents that its use would not infringe privately owned rights. References herein to any specific commercial product, process, or service by trade name, trade mark, manufacturer, or otherwise, does not necessarily constitute or imply its endorsement, recommendation, or favoring by the U.S. Government or any agency thereof. The views and opinions of authors expressed herein do not necessarily state or reflect those of the U.S. Government or any agency thereof.

ORNL/TM-2016/93

Thermodynamic and Kinetic Model Development of Thermal Segregation of Phosphorus in Iron, Fe-Cr and Fe-Ni Systems – Towards the Development of a Comprehensive Solute Segregation Model

Ying Yang

03/2016

Prepared for the
U.S. Department of Energy
Office of Nuclear Energy

ABSTRACT

Radiation induced segregation (RIS) has been frequently reported in structural materials such as austenitic, ferritic, and ferritic-martensitic stainless steels (SS) that have been widely used in light water reactors (LWRs). RIS has been linked to secondary degradation effects in SS including irradiation induced stress corrosion cracking (IASCC). Earlier studies on thermal segregation in Fe based alloys found that metalloids elements such as P, S, Si, Ge, Sn etc. embrittle the materials when enrichment was observed at grain boundaries. RIS of Fe-Cr-Ni based austenitic steels has been modeled in the U.S. 2015 fiscal year (FY2015), which identified the pre-enrichment due to thermal segregation can have an important role on the subsequent RIS. The goal of this work is to develop thermal segregation models for alloying elements in steels for future integration with RIS modeling.

Thermal segregation and RIS of P in α iron and various steels has been extensively studied and therefore has been chosen as the first element to study. Two approaches have been used for thermodynamic modeling. The first approach is an empirical approach which fitted experimental segregation data into the simple McLean equation, and obtained a composition-independent segregation energy. The second approach is based on the concept the grain boundary segregation transition (GBST). GBST is such a transition when components have strong repelling interaction, the segregation energy or driving force for solute segregation is so large that there will be sharp change from a low segregated state to a high segregated state. The second approach calculates partial molar surface energy of grain boundaries (GB) as a function of temperature and composition. When partial molar surface energy of each component equals each other, then equilibrium is reached. Unlike the first approach, the experimental segregation data is never used to fit model parameters.

The kinetics modeling coupled with thermodynamic calculation provided insight on the mechanism for P segregation. It essentially consists of two steps: on one hand, at GBs, the formation of Fe_3P and the repelling interaction between Fe and Fe_3P provided large driving force for P segregation, leading to full coverage of Fe_3P at GBs for most high P alloys under equilibrium conditions; on the other hand, the segregation is also controlled by kinetics. The transportation of P in bulk is through the diffusion of P, not the Fe_3P. The diffusion of P in bulk depends on two factors: temperature and bulk composition of P. The lower temperature and/or the higher bulk composition of P, provided larger supersaturation for segregation, therefore, the large driving force for diffusion. The fast diffusion of P in α iron in temperature greater than 700~800°C allows fast build-up of P segregation at GBs, but at low temperature (<500°C), the kinetics is very slow and the equilibrium can rarely be reached. A similar case can be applied to the low P alloy. Therefore, extra caution is needed to interpret experimental data from low temperature and low P alloys.

ACKNOWLEDGEMENTS

This work was supported by the U.S. Department of Energy (DOE), Office of Nuclear Energy, Light Water Reactor Sustainability (LWRS) Research and Development Effort, under contract DE-AC05-00OR22725 with UT-Battelle, LLC. Discussions with Drs. J.T. Busby, K. Field and K. Leonard are acknowledged.

CONTENTS

ABSTRACT iv

ACKNOWLEDGEMENTS vi

ACRONYMS xii

1. Introduction 1

2. Literature review and methodology 1
   - 2.1 Thermodynamic model 2
   - 2.2 Kinetic model 4

3. Results and discussion 5
   - 3.1 Thermodynamic and kinetic calculation of thermal segregation in Fe-P 5
     - 3.1.1 Thermodynamic calculation 5
     - 3.1.2 Kinetic calculation 6
   - 3.2 Thermodynamic and kinetic calculation of thermal segregation in Fe-Fe_3P 7
     - 3.2.1 Thermodynamic calculation 7
     - 3.2.2 Kinetic calculation 9
   - 3.3 Discussion on the approaches 10
   - 3.4 Effect of interaction energy in multicomponent systems on thermal segregation in Fe-Cr-P and Fe-Ni-P 11

4. Future work 13

5. References 15

FIGURES

Figure 1: Assumed free energy versus depth for segregant atoms at the surface and in the bulk..... 4

Figure 2: The equilibrium segregation of phosphorus at grain boundary (a) as a function of alloy composition (bulk phosphorus content) at 500°C, and (b) as a function of both alloy composition (wt%) and temperature, compared to the experimental data from Erhart and Grabke..... 6

Figure 3: The composition of P at GBs (a) at 450 ^{o}C for Fe-0.33wt%P as a function of distance from GB for the 0.1h and 10000h periods; (b) as a function of time for alloy Fe-0.33 wt%P and Fe-0.003 wt%P at 723 and 1073K (450 and 800°C), respectively. 7

Figure 4: The surface energy of Fe and Fe_3P at GB as a function of GB composition (a) for Fe-0.032at%P alloy and (b) for Fe-Xat%P (X=1e-3~1) alloys..... 8

Figure 5: The surface energy of Fe and Fe_3P at GB as a function of GB composition for alloys investigated in Erhart and Grabke's work (a) at 1073K (b) 723K..... 9

Figure 6: (a) The composition of P at GBs as a function of time for alloy Fe-0.33 wt%P and Fe-0.003 wt%P at 450 and 800°C, respectively; (b) the time to reach equilibrium segregation at 500 ^{o}C for a range of alloys. 10

Figure 7: The calculated P, Cr and Ni segregation at GB as a function of temperature for Fe-2.3Ni-0.086P, Fe-2.3Cr-0.086P and Fe-0.086P (at%) alloys. 12

ACRONYMS

SS: Stainless Steels

RIS: Radiation Induced Segregation

GB: Grain Boundary

GBST: Grain Boundary Segregation Transition

IASCC: Irradiation Induced Stress Corrosion Cracking

LWRs: Light Water Reactors sustainability

CT: Computational Thermodynamics

Thermodynamic and Kinetic Modeling on Thermal Segregation of Phosphorus in α Iron

1. Introduction

Structural materials such as austenitic, ferritic, and ferritic-martensitic stainless steels (SS) are widely used in light water reactors (LWRs). However, the combined long-term neutron irradiation and thermal conditions impose great challenges on the stability of materials. For example, a variety of microstructural and microchemical changes have been reported in austenitic SS core internals of LWRs, primarily including a high density (10^{22}–10^{23} m^3) of Frank loops (< approximately 20 nm), precipitates (e.g., Ni/Si-rich γ', G-phases and carbides), and cavities, as well as chemical segregation at grain boundaries (GBs) and dislocations [1-5]. These changes lead to material degradation such as irradiation-assisted stress corrosion cracking (IASCC). IASCC has been linked to the depletion of Cr at the grain boundary as a result of radiation-induced segregation (RIS) [2]. RIS modeling of Fe-Cr-Ni system has been subjected to several prior studies [6-13]. Recently, Yang et al. [14] has developed an improved RIS model based on Perks model [15] by integrating computational thermodynamics (CT) [16] into the modeling of compositional dependent diffusion coefficients and thermodynamic factors, and interstitial binding model [13] into the modeling diffusion flux of interstitials. One of the major findings resulted from the improved model is that the elemental segregation in the steady state is the result of not only preferential coupling of elements with defects but also the composition gradient in the vicinity of the grain boundary that was formed during the transient state. The latter is the major cause for the oscillatory behavior of segregation profile (such as a W-shape) in the vicinity of the GB. While Yang's study shows the composition gradient that formed from the transient state has an important role in the steady-state microchemistry at defect sinks, Busby et al. [17] found that the pre-existing Cr-enrichment at grain boundary due to thermal segregation also leads to the oscillatory behavior of segregation profiles during the subsequent irradiation. Similarly, Cole et al. [18] found Cr and Mo in 316SS under different cooling rates had already enriched to various levels at grain boundary before the materials being exposed to irradiation environments. The higher the enriched levels lead to the more pronounced W-shape profile during the subsequent irradiation. Nastar et al. [19] did a mean-field RIS kinetics simulation and also found a W-shape profile of Cr when using a pre-enriched Cr profile as input. It becomes evident that pre-enrichment of element at GBs due to thermal segregation has an important role in determining the subsequent RIS profile as well as the microchemistry at GBs [17-19].

Earlier studies on thermal segregation of metalloid impurities in Fe based alloys found that metalloids elements such as P, S, Si, Ge, Sn etc. embrittle the materials when they enrich at grain boundaries [20]. This work aims at developing a computational model to describe thermodynamics and kinetics of thermal segregation of alloying elements in austenitic and ferritic steels. This model will be eventually coupled with the RIS model to provide a complete description of complicated, multi-elemental segregation under both irradiation and thermal conditions.

2. Literature review and methodology

Among various elements, thermal segregation of phosphorus at GBs of ferritic alloys is one of the most widely studied subjects and has been known as a primary contributor to the temper embrittlement of low-alloying steels [21-28]. Not only thermal segregation, the irradiation

enhanced P segregation at GBs has been also connected with irradiation enhanced embrittlement of pressure vessel steels of nuclear reactors [29-35]. Therefore, thermal segregation of P was selected as the first system to be investigated using the currently developed models. While the reported experimental results on P segregation at the GB of α iron differ from one work to the other, due to the presence of other impurity elements, the different cooling rates (eg., furnace cooling or water quench) and aging periods, etc., there are general trends that can be captured from the experimental results, as summarized in the following: 1) The segregation levels of P increases proportionally with the bulk concentration; 2) The segregation levels of P decreases with the increasing aging temperature; 3) The chemical state of P at GB is dominated by Fe_3P; 4) P segregation at GBs occurs in merely a few or even only one atomic layer; 5) Both small angle and low Σ symmetric boundaries correspond to low levels of P segregation. Although the grain boundary structure has an important role in the segregation process, the current modeling will focus on thermodynamic and kinetic aspects of P segregation at random high angle GBs, where the segregation level is the greatest. The future refinement of the current models will include the GB structure modeling such as the work of Field et al. [7].

2.1 Thermodynamic model

McLean [36] developed a theory to describe the thermodynamics of equilibrium segregation. The McLean segregation equation describes the relationship between surface composition, bulk composition and segregation energy. For an A-B system, with A as the solvent and B as the solute, the surface composition is described as Eq. (1):

$$\frac{x_B^{\varphi}}{1-x_B^{\varphi}} = \frac{x_B}{1-x_B}\exp\left(\frac{\Delta G_B^{seg}}{RT}\right) \qquad (1)$$

x_B^{φ} is the surface composition and x_B is the bulk composition. ΔG_B^{seg} is the segregation energy. R is gas constant and T is temperature in Kelvin. The McLean equation has two assumptions: 1) the segregated atoms are non-interacting, and 2) the components have equal atomic size. The McLean equation is generally applied to a dilute solution where the x_B is neglible. Fowler [37] introduced interaction energy (Ω) between adjacent adsorbate atoms into segregation energy such that they attract (negative Ω) or repel (positive Ω) each other. The general formula of Fowler segregation model is described by Eq. (2):

$$\frac{x_B^{\varphi}}{1-x_B^{\varphi}} = \frac{x_B}{1-x_B}\exp\left(\frac{\Delta G_B^{Seg}+\Omega x_B^{\varphi}}{RT}\right) \qquad (2)$$

If Ω is zero, the Fowler equation reduces to the McLean equation. As Ω becomes more and more positive the segregation shows progressively sharper rises as the temperature falls until eventually the rise in segregation is discontinuous at a certain temperature. An analog is an immiscibility gap in a phase diagram. Such a discontinuity can be correlated the concept called grain boundary segregation transition (GBST) at which the solute coverage at GBs changes from a low segregated state to a high segregated state. Guttermann [23] further developed the Fowler's theory into a multicomponent system. The surface composition of a solute in a multicomponent system can be written as Eq. (3):

$$x_i^{\varphi} = \frac{x_i^{\varphi}\exp\left(\frac{\Delta G_i}{RT}\right)}{1-\sum_{i\neq M} x_i+\sum_{i\neq M} x_i\exp\left(\frac{\Delta G_i}{RT}\right)} \qquad (2)$$

"*i*" and "*M*" respectively denote alloying and matrix elements. Although the Guttmann's segregation equation resembles the McLean's one, however, there is a major difference between the McLean's and Guttmann's model. ΔG_B^{seg} in the McLean equation is independent of composition x_B^{φ}. If applying the McLean equation to a multicomponent system, the segregation energies of individual solute elements equal to those in the respective binary alloys and are independent of bulk and surface composition. However, in Guttmann's equation, the segregation energy of an individual element is a function of composition. The compositional dependency is described as Eq. (3):

$$\Delta G_i = \Delta G_i^0 + RTln\frac{f_M^{\varphi} f_i}{f_i^{\varphi} f_m} \qquad (3)$$

ΔG_i^0 is the segregation energy in the respective *M-i* binary, which is independent of composition. f_M^{φ} and f_M are the fugacity of M in surface and bulk, respectively. Similarly, f_M^{φ} and f_M are the fugacity of i in surface and bulk. The fugacity is dependent on the surface and bulk composition.

Not only the choice of segregation energy, but also the choice of the segregation system is important in describing the thermodynamics. The majority of experimental data in literature was using auger electron spectroscopy (AES), which measures the enrichment of elements at GBs. However, it cannot tell the chemical state of the elements. Suzuki et al. has used XPS to discover that the chemical state of P at GBs is in the Fe_3P state [26, 27]. Hashimoto et al. [38] used first principle calculation to derive the lowest energy state and confirmed the findings from Suzuki. Kaptay [39] recently modeled the phosphorus GB segregation based on the Fe-Fe_3P system using the Butler model [40]. The Butler's model is essentially the Guttmann's model, but originally developed for the surface tension of liquid solution. The reason Kaptay choose Fe_3P over P is because the factor that segregation usually occurs in a system with phase separation, i.e., a system with a positive mixing energy to form a solution. However, in Fe-P system, the mixing energy in body centered cubic (BCC)[Fe,P] is negative, suggesting no segregation should occur. Nevertheless, if the negative mixing energy was used to create the Fe_3P cluster, and the interaction energy between Fe and Fe_3P remains positive, then the segregation of P would occur in the form of Fe_3P. His model was able to reasonably describe the P segregation at 1450°C, and predict a grain boundary segregation transition at which point the coverage of Fe_3P goes from a low segregated state to a high segregated state. Although with favorable comparison at high temperature, the Fe-Fe_3P model was not validated by the experimental data at low temperature.

In this work, equilibrium segregation was modeled using two approaches: The first approach dealt with the Fe-P system and fitted experimental segregation data into the simple McLean equation, from which composition-independent segregation energy can be obtained. The second approach dealt with the Fe-Fe_3P system, and is based on the concept the grain boundary segregation (GBST). Diffusion modeling of P was then coupled with thermodynamic modeling in both approaches to describe the kinetics of P segregation. Finally, preliminary modeling based on the Fowler/Guttmann's model was also performed to understand the effect of ternary interaction energy on the equilibrium segregation in the Fe-Cr-P and Fe-Ni-P system.

2.2 Kinetic model

Materials thermodynamics dictated the maximum solute segregation at GBs, however, it cannot tell us how long for the system to reach the maximum segregation. In this work, we also developed a kinetic model based on foreign atom movement in an appropriate potential, which aims at giving a consistent description of the segregation equilibria, the time and temperature dependence of surface concentration and in-depth concentration distribution. The frame work of kinetic models is referenced to the work by Hofmann and Erlewein [41]. Only some basic equations and information are described here. The model assumes negligible interface evaporation and the GB enrichment limited to the first monolayer. The potential gradient for GB segregation adopted from Hofmann and Erlewein's work is schematically shown in Figure 1.

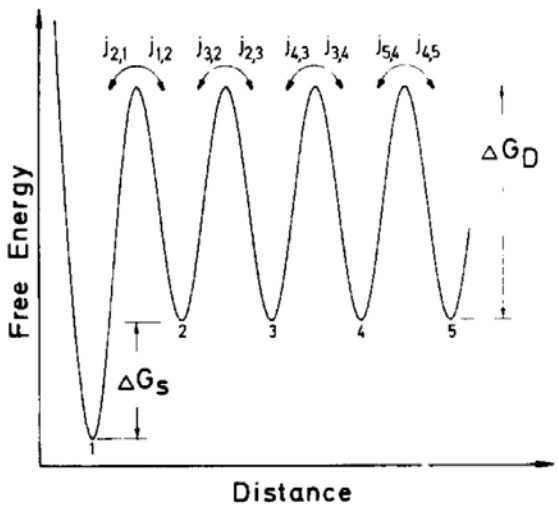

Figure 1: Assumed free energy versus depth for segregant atoms at the surface and in the bulk

Atomic fluxes based on reaction rate theory were used to describe the attainment of concentration distribution, avoiding difficulties with the solution of a diffusion equation in a potential gradient. The flux equations were described by Eq. (4a~d):

$$J_{12} = a_1^{-2} X_1 W_{12} \vartheta_1 \exp\left[-\frac{\Delta G_D - \Delta G_S}{RT}\right] \qquad (4a)$$

$$J_{21} = a_1^{-2} X_2 W_{21} \vartheta_2 \exp\left[-\frac{\Delta G_D}{RT}\right] \qquad (4b)$$

$$J_{23} = a_1^{-2} X_2 W_{23} \vartheta_2 \exp\left[-\frac{\Delta G_D}{RT}\right] \qquad (4c)$$

…

$$J_{i,i+1} = a_i^{-2} X_i W_{i,i+1} \vartheta_i \exp\left[-\frac{\Delta G_D}{RT}\right] \qquad (4d)$$

Where a_i is the atomic jump distance, X_i is the concentration of solute atoms in layer "i", ϑ_i is the solute atom oscillation frequency and $W_{i,i+1}$ is the jump probability factors of the solute atoms. In a first order approximation, all jump frequencies are assumed to be equal as well as the jump distances. The deviation for a_1 and $\vartheta_1$from this assumption will be accounted by segregation energy. ΔG_D is the activation energy for diffusion, and it will be derived from the experimental diffusion coefficient. ΔG_S is the segregation energy, which will be derived from

either experimental data or the thermodynamic theory discussed in Section 2.1. The jump probability factor was assigned using the following relationship based on Hofmann's work:

$$w_{21} = (1 - \frac{X_S}{X_S^M})^{X_S^M} \quad (5a)$$

$$W_{12} = 1 - X_2 \ (5b)$$

$$W_{23} = 1 - X_3 \ (5c)$$

$$W_{i,i+1} = 1 - X_{i+1} \ (5d)$$

Where X_S is surface composition and X_S^m is the maximum allowable surface coverage

Computational codes for calculating thermodynamics and kinetics of thermal segregation have be implemented using the wolfram programing language and the Matlab.

3. Results and discussion

In this section, modeling results will be presented in the following sequence: 1) thermodynamic and kinetic calculation of thermal segregation in Fe-P; 2) thermodynamic and kinetic calculation of thermal segregation in Fe-Fe_3P; 3) thermodynamic calculation of Fe-Cr-P and Fe-Ni-P.

3.1 Thermodynamic and kinetic calculation of thermal segregation in Fe-P

3.1.1 Thermodynamic calculation

Erhart and Grabke systematically studied P segregation in Fe-P, Fe-Cr-P, Fe-C-P and Fe-Cr-C-P systems [22]. The samples were made from melting high purity elements, solutionized at 1050°C for 1h, followed by water quench, tempering treatment at 850°C for 1h, and then furnace-cooled to the aging temperature. The specimens were held at the aging temperature for different periods of time and then water quenched for AES analysis. The AES analysis was done at the GBs interfaces which were obtained through fracturing at -120°C. The GB composition was derived from the peak ratio of P and Fe, which has been described in detail [42]. Based on the experimental measured GB compositions, and assuming no chemical interaction between elements, they were able to derive the segregation energy of P at GBs of α iron as -34300-21.5*T J/mol, by fitting the experimental data back into Eq. (1). The segregation energy so derived is independent of the bulk and surface composition. The calculated phosphorus composition at GBs is plotted as a function of alloy composition and temperature in Figure 2(a) and (b), compared well with the experimental data from Erhart and Grabke. The results calculated from thermal segregation models suggested that the segregation of P at GB increases with increasing bulk composition and decreasing temperature, which is in good agreement with experimental observation. The good agreement is not surprising since the segregation energy (-34300-21.5*T J/mol) was obtained through the fitting with experimental data.

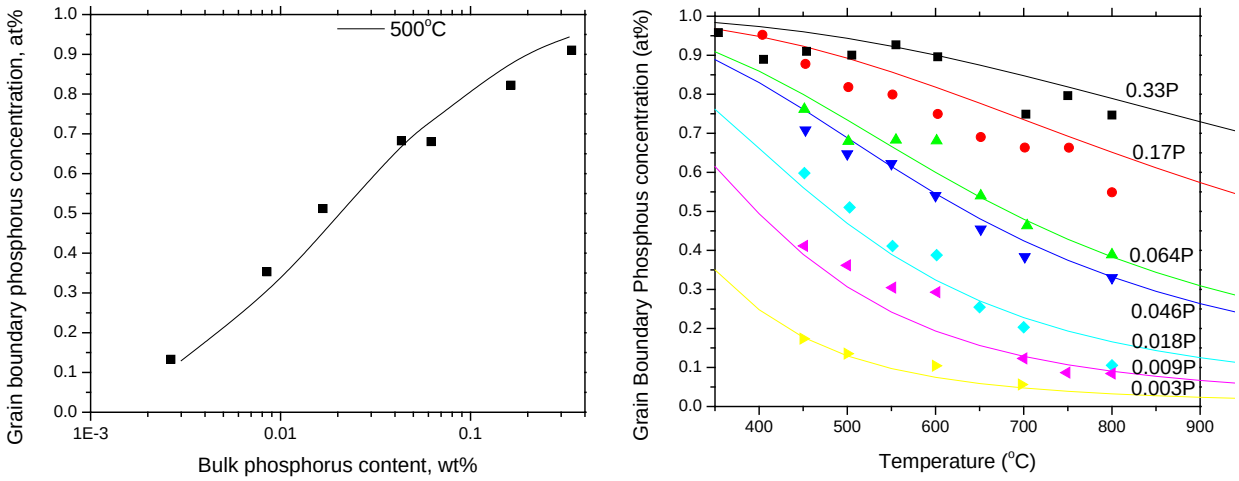

Figure 2: The equilibrium segregation of phosphorus at grain boundary (a) as a function of alloy composition (bulk phosphorus content) at 500°C, and (b) as a function of both alloy composition (wt%) and temperature, compared to the experimental data from Erhart and Grabke.

3.1.2 Kinetic calculation

The kinetic simulation were performed for the alloys in Sec. 3.1.1. Based on the model description in Sec. 2.2. The most important input quantities are the diffusion coefficient of P in α iron and the GB segregation energy. The same segregation energy -34300-21.5*T J/mol was used in kinetic simulation. The phosphorus diffusion coefficient in α Fe has been measured experimentally, i.e., $1.38*10^5$ exp(-3.4 eV/kT) cm^2/s in the temperature range (932– 1017 K) and $8*10^5$ exp(-3.2 eV/kT) cm^2/s in the temperature range (783– 923 K) [43]. The P diffusion is much larger than the self-diffusion coefficient. Indeed, at 870 K, the self-diffusion coefficient is 10^{-20} m^2/s, while the diffusion coefficient of P in ferromagnetic BCC Fe is 10^{-17} m^2/s [43]. This fact could be associated with diffusion involving interstitials rather than vacancies. Domain and Besquart did ab-initio calculation on the diffusion of P in α iron [44]. They found that the diffusion coefficient of P based on a vacancy mechanism, although less than the experimental measurement of P in α iron, had already been larger than the self-diffusion coefficient by one to three orders of magnitude. Due to the lack of quantitative description of the interstitial diffusion of P in α iron, we will use experimental diffusion coefficient data of P in α iron in this work. We had simulated the GB composition of P as a function time, temperature, and bulk composition. Critical results are now presented.

For an alloy with a high P composition of 0.33 wt% P at 723K(450°C), the calculated concentration profile of P as a function of distance from GB is plotted in Figure 3 (a). The red curve denotes the profile at 0.1h and the blue curve at 10000h. The results suggested at the earlier stage of segregation, there is a depletion regime of P at the sub-GB region. This is because the segregation energy leads to a large flux from sub-GB region to GB plane, while at this time, the flux into the sub-GB regime was supplied by continuous diffusion from the bulk. For longer times, the GB segregation gradually reaches equilibrium, and the depleted region gradually disappears until the steady state is established.

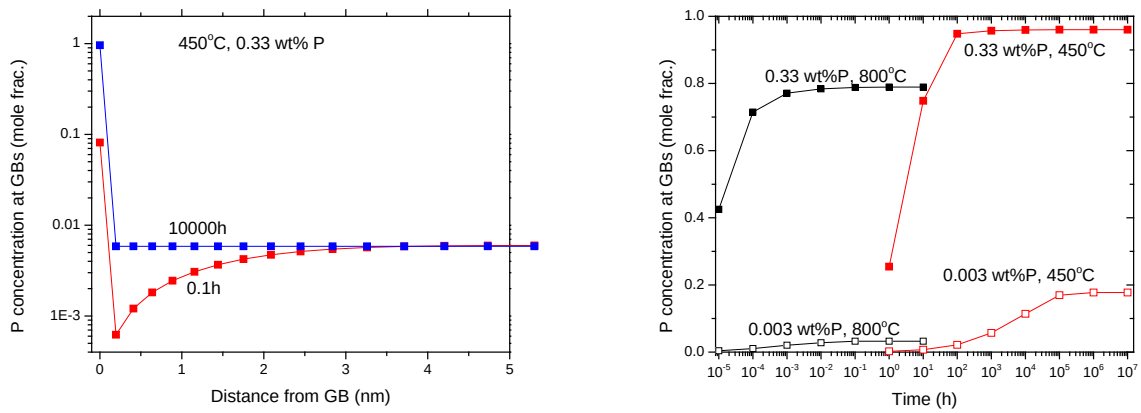

Figure 3: The composition of P at GBs (a) at 450 °C for Fe-0.33wt%P as a function of distance from GB for the 0.1h and 10000h periods; (b) as a function of time for alloy Fe-0.33 wt%P and Fe-0.003 wt%P at 723 and 1073K (450 and 800°C), respectively.

In Figure 3(b), the P composition at GBs as a function of time was calculated for Fe-0.33wt%P and Fe-0.003wt% P alloys at 723 and 1073K (450 and 800°C), respectively. The plateau in each curve suggests the equilibrium segregation is reached. The results show that the equilibrium segregation at 800°C is reached within 0.01~0.1h, while the time to reach equilibrium at 723K(450°C) is 10^3 h for high P alloy and 10^6 h for low P alloy. The equilibrium segregation level predicted from the kinetic modeling is well consistent with the thermodynamic calculation in Figure 2 (b), indicating the self-consistence of the two models. However, based on the kinetic simulation, an immediate question is whether the experimental data at 723K(450°C) obtained from Erhart and Grabke's work [22] were truly reaching equilibrium segregation values. Although they didn't give the annealing time for alloys at each temperature, it is impossible for the annealing time to be 10^6 h. Even 10^3 h for the high P alloy is unlikely. Therefore, the segregation data for low temperature and low P alloys in Erhart and Grabke's work are considered as non-equilibrium segregation, and the segregation energy derived from these data are also questionable.

3.2 Thermodynamic and kinetic calculation of thermal segregation in Fe-Fe_3P

3.2.1 Thermodynamic calculation

Modeling P segregation at GBs based on the Fe-Fe_3P system follows the work done by Kaptay [39]. The goal on one hand is to reproduce the calculated results for high temperature (1723K), on the other hand to predict the segregation at low temperature (723K ~1073K) where the experimental data from Erhart and Grabke's work can be compared. All the parameters and equations have been described in detail in Kaptay's work, and therefore only critical information are listed here. In the McLean's equation, the surface energy of GB is implicitly included in Eq. (1). While in Kaptay's approach (based on Bulter's equation), the surface energy was explicitly described as Eq. (4)

$$\sigma_i = \sigma_i^0 + \frac{RT}{\omega_i}\ln\left(\frac{x_i^\varphi}{x_i}\right) + \frac{\Delta G_i^{E,\varphi} - \Delta G_i^E}{w_i} \qquad (6)$$

$$\Delta G_i^\varphi = RTln\left(x_i^\varphi\right) + \Delta G_i^{E,\varphi} \qquad (7)$$

$$\Delta G_i = RTln(x_i) + \Delta G_i^E \qquad (8)$$

σ_i^0 is the surface energy of pure element i. ω_i is the molar interfacial energy. $\Delta G_i^{E,\varphi}$ and ΔG_i^E are the partal molar excess mixing Gibbs energy of component "*i*" in the GB and bulk region, respectively. It should be noted the "*i*" now is referred to Fe and Fe_3P, respectively. X_{Fe3P} is the composition of Fe_3P cluster, which can be derived from the P composition in alloy if assuming all P was used to form Fe_3P cluster. Assuming regular solution, the excess energy are described as Eqs. (7~8):

$$\Delta G_i^{E,\varphi} = \beta\Omega(1 - x_i^{\varphi})^2 \qquad (10)$$

$$\Delta G_i^E = \Omega(1 - x_i)^2 \qquad (11)$$

β is the ratio of unbroken bonds in the GB region compared to the bulk grain. Using the parameters in Kaptay's work, for an alloy Fe-0.032at%Fe_3P at 1723K, the surface energy of Fe and Fe_3P at GB is plotted as a function of GB composition, as shown in Figure 4 (a). The red curve is for Fe_3P and the black is for Fe. These two curves have only one intersecting point, which is σ=0.81 J/m^2 and the X_{Fe3P}=0.075. Only at this point, the partial surface energy of Fe and Fe_3P are equal, i.e., satisfying the equilibrium condition. Therefore, the equilibrium GB segregation composition of P for this alloy at 1723K is 0.075. We then did this calculation for a range of alloys with different Fe_3P concentration at the same temperature. The calculation results shown in Figure 4 (b) suggest that the composition of P at GBs sharply changes from a low segregated level in Fe-0.032at%Fe_3P to a high segregated level in Fe-0.1at%Fe_3P. In other words, the equilibrium composition of Fe_3P at GBs are less than 0.075 for alloys with Fe_3P composition less than or equal to 3.2e-4, and greater than 0.9 for alloys with Fe_3P composition over or equal to1e-3. The Fe_3P composition corresponding to the GBST at 1723K is calculated as 0.0004. This result agrees well with the simulation results of Kaptay and experimental results by Hondros et al.[25].

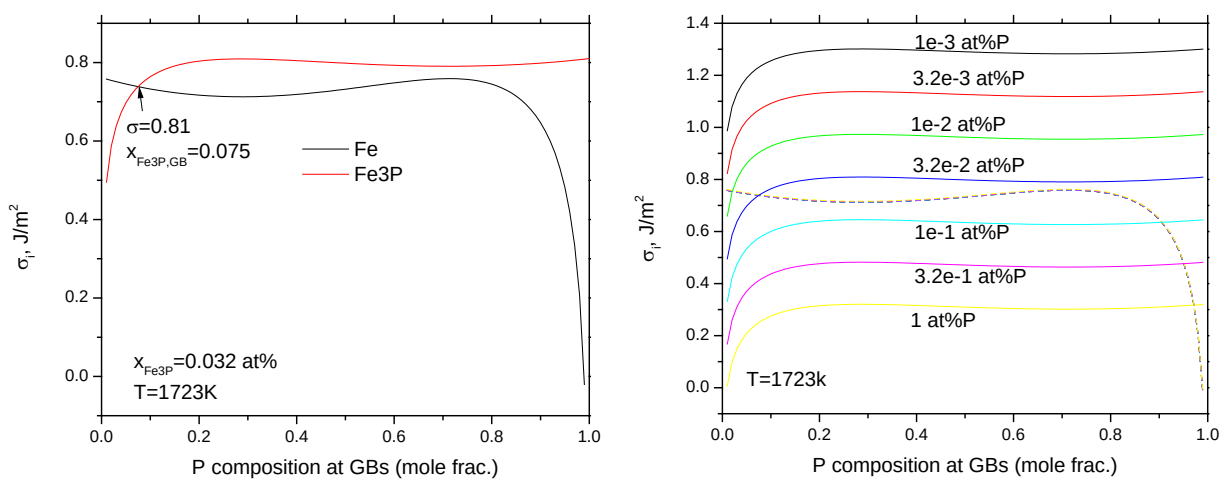

Figure 4: The surface energy of Fe and Fe_3P at GB as a function of GB composition (a) for Fe-0.032at%P alloy and (b) for Fe-Xat%P (X=1e-3~1) alloys

Next, this approach was used to predict the GB segregation of Fe-Fe_3P at a temperature range from 1073K to 723K. At 1073K, the GBST occurs in between 0.009 wt% P, while at 723K, all

alloys are in high segregated states. These calculation results suggest that most alloys investigated by Erhart and Grabke's at temperature (1073~723K) are almost fully covered by Fe_3P, if equilibrium segregation can be reached. These results can be understood by analogy with the immiscibility gap case. At low temperature, the solubility of a solute in the solvent-rich phase is lower than that at high temperature, therefore, an alloy can easier surpass the solubility to form the solute rich phase at low temperature than at high temperature. Similarly, the GB segregation can easier to transform to the solute rich (highly segregated state) at low temperature. The modeling correctly reflected such a trend, suggesting the models are sensible. However, it should be noted that among many parameters used by Kaptay, two parameters have great uncertainties and subsequently exert great influence on the calculation results. One is the surface energy of pure Fe_3P and the other is solubility of Fe_3P in Fe. The latter one mainly affects the interaction energy used for the modeling. While the current work is a preliminary step to test the modeling code, future work on testing the sensibility of these parameters are needed.

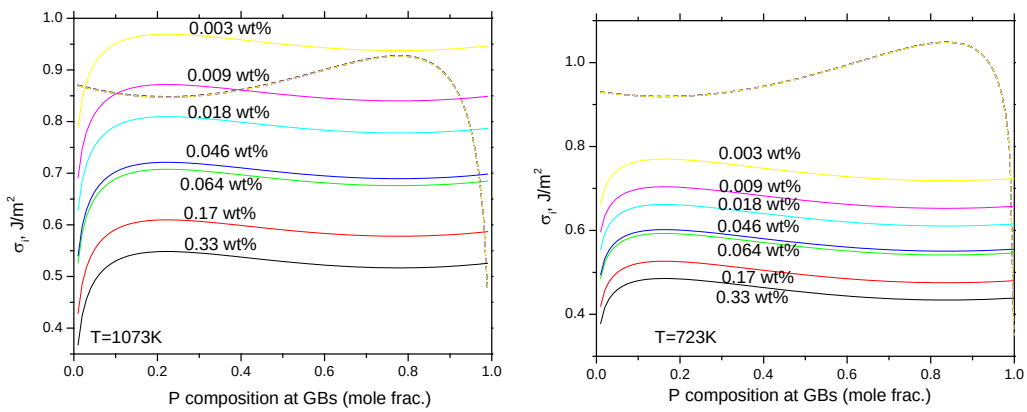

Figure 5: The surface energy of Fe and Fe_3P at GB as a function of GB composition for alloys investigated in Erhart and Grabke's work (a) at 1073K (b) 723K

3.2.2 Kinetic calculation

In Section 3.2.1, the composition of P at GBs is nearly full coverage when equilibrium is reached. Now, we want to find out how long for the system to reach equilibrium. The same experimental diffusion coefficient of P in α iron at that in Sec. 3.1.2 is used. The segregation energy in Kaytay's approach can be described as Eq. (12):

$$\Delta G^{seg} = \sigma * (\omega_{Fe3P} - \omega_{Fe}) - (\sigma^0_{Fe3P} * \omega_{Fe3P} - \sigma^0_{Fe} * \omega_{Fe}) - \Omega(\beta\left(1 - 2x^{\varphi}_{Fe3P}\right) - (1 - 2x_{Fe3P})) \qquad (12)$$

Now, the segregation energy is dependent on the composition of P in both GB and bulk region. Substituting this equation into the boundary condition for kinetic model, the kinetics of P segregation at GB for the alloys in Erhart and Grabke's work are calculated and presented below.

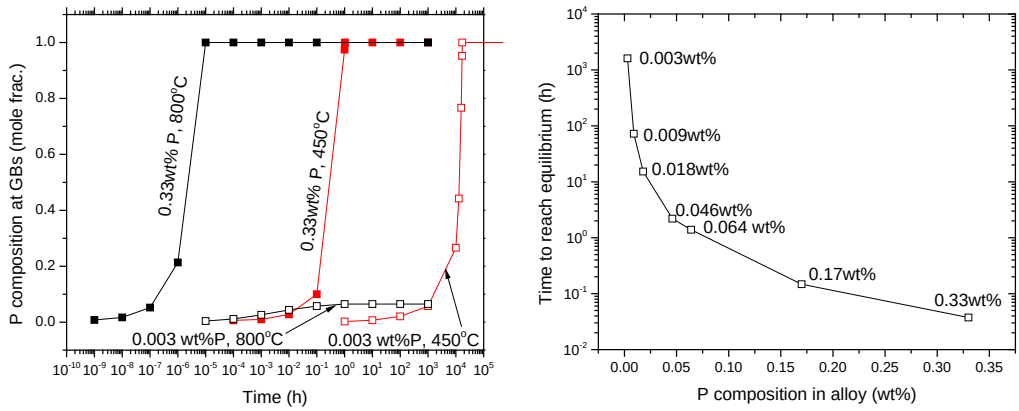

Figure 6: (a) The composition of P at GBs as a function of time for alloy Fe-0.33 wt%P and Fe-0.003 wt%P at 450 and 800°C, respectively; (b) the time to reach equilibrium segregation at 500 ^{o}C for a range of alloys.

In Figure 6(a), the P composition at GBs as a function of time was calculated for Fe-0.33 wt% P and Fe-0.006 wt% P alloys at 450 and 800°C, respectively. The plateau in each curve suggests the equilibrium segregation is reached. The composition of P at GBs of the high P alloy (Fe-0.33wt% P) is always 1, no matter at 800 or 450°C, indicating the grain boundary is completely covered by Fe_3P. In correlation to the thermodynamic calculation in Figure 5, the 0.33 wt% P is greater than GBST composition of Fe-P alloys at both 800 and 450°C, therefore, the grain boundary enrichment of P is on the highly-segregated state. On the other hand, the equilibrium composition of P in the Fe-0.003 wt% P alloy at 800°C is 0.0648, suggesting the 0.003 wt% P is lower than the GBST composition, therefore, the GB segregation is in the low-segregated state. This is consistent with the thermodynamic calculation in Figure 5. However, as the P solubility in α iron decreases with temperature, therefore, the Fe-0.003wt%P alloy at low 450°C is greater than the GBST composition, therefore, its equilibrium segregation at GBs is in high segregated state. Figure 6 (b) plots the needed time for the alloys in Erhart and Grabke's work to reach equilibrium at 500°C. The time increases with degreasing bulk P composition. With these results, we would like to discuss the trend found by Erhart and Grabke. In their work, they found that the GB enrichment increases with decreasing temperatures. While this is correct from pure thermodynamic analysis, this might not be the reason for their results. Their observed GB enrichment is influenced by both thermodynamic and kinetics, especially when different temperature and bulk compositions are involved. Take the Fe-0.003 wt% P alloy as an example, the low enrichment at 800°C is due to thermodynamics as kinetics is very fast at this temperature. However, at 450°C, the equilibrium GB composition should be close to 1 while their measurement is only 18%.

3.3 Discussion on the approaches

The first approach is an empirical approach which fitted experimental segregation data into the simple McLean equation, and obtained a composition-independent segregation energy. At first sight, it seems that the calculated equilibrium segregation from this segregation can reproduce most of experimental data. However, the kinetic simulation discovered that equilibrium segregation of some low P alloys at low temperature would take 10^5~10^6 hours to reach equilibrium. The diffusivity equation used for kinetic simulation is reasonable as it correctly predicts the time for sample to reach equilibrium at 800°C is in the order of 0.1~1h.

The important message from this work is that the experimental data Erhart and Grabke's work that were used to fit the equilibrium segregation energy are quite possibly not true equilibrium data. Therefore, the segregation energy derived from this data is questionable. In addition, as this approach is an empirical approach, it cannot give us insight on the segregation mechanism behind the experimental data.

The second approach is based on the GBS concept. By analogy with the concept of immiscibility gap, for a system with a positive mixing energy, it has a nature tendency to form phase separation. GBST is such a transition when atoms have strong repelling interaction (For example, Fe and Fe_3P, they have negligible mutual solubility and do not want to mix with each other), the segregation energy for the solute is large, driving strong GB segregation. At certain composition, the driving force is so large that there will be sharp change from low segregated state to high segregated state (i.e., GBST). The second approach calculates partial molar surface energy of GB as a function of temperature and composition. When partial molar surface energy of each component equals to each other, the equilibrium is reached. Unlike the first approach, the experimental segregation data is never used to fit model parameters, such as segregation energy, etc. On the other hand, it is necessary to have some thermodynamic and thermophysical knowledge of pure components to calculate the surface energy. Although there are some estimation methods and literature data available, these data are still largely lack. Here would be a greater opportunity for Ab-initio method to fill the gap.

The kinetics modeling coupled with thermodynamic calculation in the second approach suggested that the mechanism for P segregation consists of two steps. On one hand, at GBs, the formation of Fe_3P and the repelling interaction between Fe and Fe_3P provided large driving force for P segregation, leading to full coverage of Fe_3P at GBs for most high P alloys under equilibrium conditions; on the other hand, the segregation is also controlled by kinetics. The transportation of P in bulk is through the diffusion of P, not the Fe_3P. The diffusion of P in bulk depends on two factors: temperature and bulk composition of P. The lower temperature and/or the higher bulk composition of P, provided larger supersaturation for segregation, therefore, the large driving force for diffusion. The fast diffusion of P in α iron in temperature greater than 700~800°C allows fast build-up of P segregation at GBs, but at low temperature (<500°C), the kinetics is very slow and the equilibrium can rarely be reached. Similar case can be applied to the low P alloy. Therefore, extra cautiousness is needed to interpret experimental data from low temperature and low P alloys.

3.4 Effect of interaction energy in multicomponent systems on thermal segregation in Fe-Cr-P and Fe-Ni-P

While Erhart and Grabke fitted their experimental data into the simple McLean equation and obtained a composition independent segregation energy, we had tried to fit their data into Flower and Guttermann's equation, where the chemical interaction energy from binary and ternary was included. The goal was to examine when binary interaction in Fe-P is replaced by binary and ternary interaction in Fe-Cr-P and Fe-Ni-P systems, how the segregation would response. This work is done before the kinetic modeling, therefore, non-equilibrium effect wasn't considered in the analysis below. Although the analysis cannot be for any quantitative prediction, it can help us to understand the role of the ternary interaction. The key to this study is to describe the total

segregation energy of element in ternary system $\Delta G_I = \Delta G_I^o + \Delta G_I^E$. The first part is due to strain energy as described in the McLean segregation equation.

While the value for this term for P can be derived from the binary Fe-P system, that for Cr was not well experimentally studied. Therefore, the value for Cr is assumed as two levels, one is 1 kJ/mol, which is essentially negligible compared with that of P (34300+21.5*T (J/mol)); the other is 10 kJ, which is in the same order of magnitude as that of P. The second part is the excess energy due to chemical interaction among Fe, Cr and P, the numerical value of which can be derived from thermodynamic database OCTANT [45]. This calculated segregation of P and Cr in Fe-2.3Ni-0.086P (at%) is plotted in Figure 7, together with experimental data by Erhart and Grabke [42]. The P segregation of Fe-0.086P (at%) is also plotted for comparison. The results suggested that the binary interaction between Fe and Cr as well as Cr and P, and the ternary interaction among Fe-Cr-P does not have significant effect on the segregation of P at the selected segregation energies. It was also found that the Cr at GB becomes depleted with increasing P concentration at GB, suggesting that P does have an effect on the Cr segregation. The simulated results are in reasonable agreement with experimental data.

The similar methodology has been applied to the Fe-Ni-P system. The same two level of segregation energies of Ni as that of Cr have been used, i.e., 1 kJ/mol and 10kJ/mol, due to the lack of experimental data. The results of Fe-Ni-P are plotted in Figure 7 together with Fe-Cr-P. The chemical interaction energy between Ni and P, as well as Fe and Ni, and the ternary interaction among Fe, Ni, and P was included for simulation. The calculated segregation of P and Ni in Fe-2.3Ni-0.086P (at%) suggested that Ni behaves similar to that of Cr for given segregation energies. The chemical interaction between Ni and P does not differ from that between Cr and P significantly. Both Cr and Ni do not have significant effect on the segregation of P at the selected segregation energies.

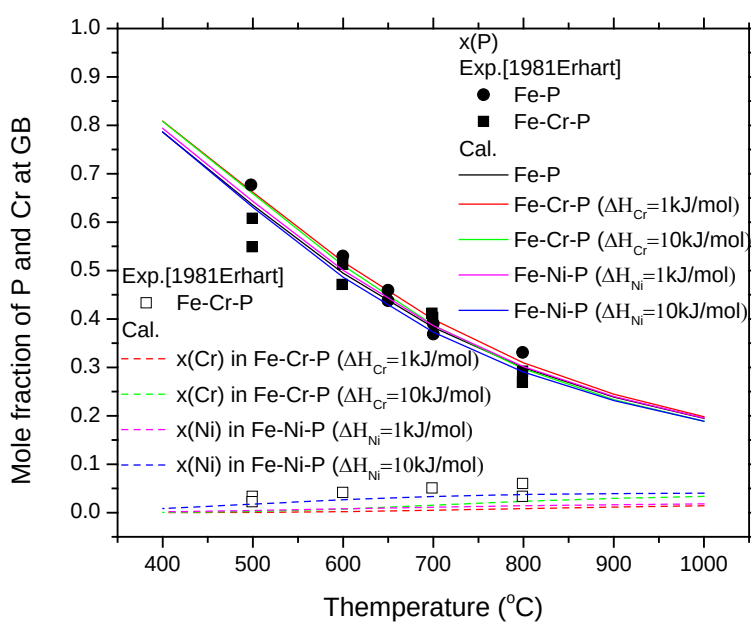

Figure 7: The calculated P, Cr and Ni segregation at GB as a function of temperature for Fe-2.3Ni-0.086P, Fe-2.3Cr-0.086P and Fe-0.086P (at%) alloys.

4. Future work

The following work is planned in the next step:

1) Additional sensitivity test on the parameters used in Approach II will be performed. Write an article on "Thermodynamic and kinetic modeling on GB segregation of P in α Iron" for Journal publication.
2) Extend the Approach II to the Fe-P-X ternary (X=Cr, Ni, Mo, Nb and Ti, etc).
3) Integrate the thermal segregation code with irradiation-induced segregation code to simulation segregation of steels used in nuclear reactors.

5. References

1. Allen, T. and J. Busby, *Radiation damage concerns for extended light water reactor service*. JOM, 2009. **61**(7): p. 29-34.
2. Fukuya, K., *Current understanding of radiation-induced degradation in light water reactor structural materials.* Journal of Nuclear Science and Technology, 2013. **50**(3): p. 213-254.
3. Garner, F., *4.02-Radiation Damage in Austenitic Steels,"*. 2012, Oxford: Elsevier. p. 33-95.
4. Kenik, E.A. and J.T. Busby, *Radiation-induced degradation of stainless steel light water reactor internals.* Materials Science and Engineering: R: Reports, 2012. **73**(7): p. 67-83.
5. Zinkle, S.J. and G. Was, *Materials challenges in nuclear energy.* Acta Materialia, 2013. **61**(3): p. 735-758.
6. Allen, T.R. and G. Was, *Modeling radiation-induced segregation in austenitic Fe–Cr–Ni alloys.* Acta materialia, 1998. **46**(10): p. 3679-3691.
7. Field, K.G., et al., *Defect sink characteristics of specific grain boundary types in 304 stainless steels under high dose neutron environments.* Acta Materialia, 2015. **89**: p. 438-449.
8. Hashimoto, T., Y. Isobe, and N. Shigenaka, *A model for radiation-induced segregation in fcc binary alloys.* Journal of nuclear materials, 1995. **225**: p. 108-116.
9. Lam, N., *Compositional changes in Fe-Cr-Ni alloys under proton bombardment at elevated temperatures.* Journal of Nuclear Materials, 1983. **117**: p. 106-112.
10. Marwick, A., *Segregation in irradiated alloys: the inverse Kirkendall effect and the effect of constitution on void swelling.* Journal of Physics F: Metal Physics, 1978. **8**(9): p. 1849.
11. Takahashi, H. and N. Hashimoto, *Radiation-induced segregation and grain boundary migration in Fe–Cr–Ni model alloy under irradiation.* Materials Transactions, JIM, 1993. **34**(11): p. 1027-1030.
12. Watanabe, S., et al., *Quantitative studies of irradiation-induced segregation and grain boundary migration in Fe Cr Ni alloy.* Journal of nuclear materials, 1995. **224**(2): p. 158-168.
13. Wiedersich, H., P. Okamoto, and N.Q. Lam, *A theory of radiation-induced segregation in concentrated alloys.* Journal of Nuclear Materials, 1979. **83**(1): p. 98-108.
14. Yang, Y.F., Kevin; Allen, Todd; and Busby, Jeremy, *Roles of Vacancy/Interstitial Diffusion and Segregation in the Microchemistry at Grain Boundaries of Irradiated Fe-Cr-Ni alloys*, Journal of Nuclear materials, 2016. **In press**.
15. Perks, J., A. Marwick, and C. English, *A computer code to calculate radiation-induced segregation in concentrated ternary alloys.* 1986.
16. Lukas, H.L., S.G. Fries, and B. Sundman, *Computational thermodynamics: the Calphad method*. Vol. 131. 2007: Cambridge university press Cambridge.
17. Busby, J., et al. *Influence of initial grain boundary composition on the evolution of radiation-induced segregation profiles*. in *MRS Proceedings*. 1998. Cambridge Univ Press.
18. Cole, J.I., et al. *The Influence of Pre-Irradiation Heat Treatments on Thermal Non-Equilibrium and Radiation-Induced Segregation Behavior in Model Austenitic Stainless Steel Alloys*. in *Effects of Radiation on Materials: 21st International Symposium*. 2004. ASTM International.
19. Nastar, M. and F. Soisson. *Radiation-induced segregation*. 2012. Elsevier B.V.
20. McMahon Jr, C. and L. Marchut, *Solute segregation in iron-based alloys.* Journal of Vacuum Science & Technology, 1978. **15**(2): p. 450-466.
21. Briant, C. and R. Mulford, *Surface segregation in austenitic stainless steel.* Metallurgical Transactions A, 1982. **13**(5): p. 745-752.
22. Erhart, H. and H. Grabke, *Equilibrium segregation of phosphorus at grain boundaries of Fe–P, Fe–C–P, Fe–Cr–P, and Fe–Cr–C–P Alloys.* Metal Science, 1981. **15**(9): p. 401-408.
23. Guttmann, M., P. Dumoulin, and M. Wayman, *The thermodynamics of interactive co-segregation of phosphorus and alloying elements in iron and temper-brittle steels.* Metallurgical Transactions A, 1982. **13**(10): p. 1693-1711.

24. Hänsel, H. and H.J. Grabke, *Grain boundary segregation of phosphorus and carbon in ferritic iron.* Scripta metallurgica, 1986. **20**(11): p. 1641-1644.
25. Hondros, E. *The influence of phosphorus in dilute solid solution on the absolute surface and grain boundary energies of iron*. in *Proceedings of the Royal Society of London A: Mathematical, Physical and Engineering Sciences*. 1965. The Royal Society.
26. Suzuki, S., K. Abiko, and H. Kimura, *Phosphorus segregation related to the grain boundary structure in an Fe□P alloy.* Scripta Metallurgica, 1981. **15**(10): p. 1139-1143.
27. Suzuki, S., et al., *Effect of carbon on the grain boundary segregation of phosphorus in α-iron.* Scripta metallurgica, 1983. **17**(11): p. 1325-1328.
28. Viswanathan, R., *Temper embrittlement in a Ni-Cr steel containing phosphorus as impurity.* Metallurgical Transactions, 1971. **2**(3): p. 809-815.
29. Brimhall, J., D. Baer, and R. Jones, *Effect of irradiation on phosphorus segregation.* Journal of Nuclear Materials, 1983. **117**: p. 218-223.
30. Druce, S.G., et al. *The modelling of irradiation-enhanced phosphorus segregation in neutron irradiated reactor pressure vessel submerged-arc welds*. in *Effects of Radiation on Materials: 17th International Symposium*. 1996. ASTM International.
31. Faulkner, R., et al., *Grain boundary segregation under neutron irradiation in dilute alloys.* Journal of nuclear materials, 1998. **255**(2): p. 189-209.
32. Gurovich, B., et al., *Intergranular and intragranular phosphorus segregation in Russian pressure vessel steels due to neutron irradiation.* Journal of nuclear materials, 2000. **279**(2): p. 259-272.
33. Nishiyama, Y., et al., *Effects of neutron-irradiation-induced intergranular phosphorus segregation and hardening on embrittlement in reactor pressure vessel steels.* Acta Materialia, 2008. **56**(16): p. 4510-4521.
34. Song, S.-H., et al., *Grain boundary phosphorus and molybdenum segregation under irradiation and thermal conditions in a 2.25 Cr1Mo steel.* Materials Science and Engineering: A, 2000. **286**(2): p. 230-235.
35. Watanabe, H., et al., *Effects of phosphorus on defect behavior, solute segregation and void swelling in electron irradiated Fe□Cr□Ni alloys.* Journal of Nuclear Materials, 1988. **155**: p. 815-822.
36. Guttmann, M., et al., *Interfacial segregation.* ASM, Metals Park, OH, 1979: p. 261.
37. Fowler, R.H. and E.A. Guggenheim, *Statistical thermodynamics.* 1941.
38. Hashimoto, M., et al., *Atomistic studies of grain boundary segregation in Fe-P and Fe-B alloys—I. Atomic structure and stress distribution.* Acta Metallurgica, 1984. **32**(1): p. 1-11.
39. Kaptay, G., *Modelling equilibrium grain boundary segregation, grain boundary energy and grain boundary segregation transition by the extended Butler equation.* Journal of Materials Science, 2016. **51**(4): p. 1738-1755.
40. Wang, N., J.P. Butler, and D.E. Ingber, *Mechanotransduction across the cell surface and through the cytoskeleton.* Science, 1993. **260**(5111): p. 1124-1127.
41. Hofmann, S. and J. Erlewein, *A model of the kinetics and equilibria of surface segregation in the monolayer regime.* Surface Science, 1978. **77**(3): p. 591-602.
42. Grabke, H., et al., *Effects of manganese on the grain boundary segregation, bulk and grain boundary diffusivity of P in ferrite.* Scripta metallurgica, 1987. **21**(10): p. 1329-1334.
43. Le Claire, A. and G. Neumann, *Diffusion of Impurities in Solid Metallic Elements, Chap. 3 in: Diffusion in Solid Metals and Alloys, H. Mehrer (Vol. Ed.), Landolt-Börnstein, Numerical Data and Functional Relationships in Science and Technology, New Series Vol. III/26*. 1990, Springer-Verlag.
44. Domain, C. and C. Becquart, *Diffusion of phosphorus in α− Fe: An ab initio study.* Physical Review B, 2005. **71**(21): p. 214109.
45. Yang, Y. and J.T. Busby, *Thermodynamic modeling and kinetics simulation of precipitate phases in AISI 316 stainless steels.* Journal of Nuclear Materials, 2014. **448**(1): p. 282-293.